

# Effect of Pupil Dilation and Constriction on the Distribution of Bit Errors within the Iris

Inmaculada Tomeo-Reyes

Queensland University of Technology

2 George St., Brisbane, QLD, 4000, Australia

inma.tomeoreyes@qut.edu.au

Vinod Chandran

Queensland University of Technology

2 George St., Brisbane, QLD, 4000, Australia

v.chandran@qut.edu.au

## Abstract

*Texture information in the iris image is not uniform in discriminatory information content for biometric identity verification. The bits in an iris code obtained from the image differ in their consistency from one sample to another for the same identity. In this work, errors in bit strings are systematically analysed in order to investigate the effect of light-induced and drug-induced pupil dilation and constriction on the consistency of iris texture information. The statistics of bit errors are computed for client and impostor distributions as functions of radius and angle. Under normal conditions, a V-shaped radial trend of decreasing bit errors towards the central region of the iris is obtained for client matching, and it is observed that the distribution of errors as a function of angle is uniform. When iris images are affected by pupil dilation or constriction the radial distribution of bit errors is altered. A decreasing trend from the pupil outwards is observed for constriction, whereas a more uniform trend is observed for dilation. The main increase in bit errors occurs closer to the pupil in both cases.*

## 1. Introduction

The human iris contains rich texture information determined by distinctive features such as furrows, crypts, and ridges. The randomness in the texture content, together with its uniqueness and stability make it possible to use the iris pattern as a highly reliable method for recognition of individuals [1]. However, texture information within the iris is not equally consistent.

Different approaches have been considered in the literature to identify the location of the most discriminatory information of the iris. An early approach proposed by Pereira and Veiga [2] analysed all possible combinations of five out of ten concentric rings of the iris region to improve the performance of an iris recognition system. To complete their analysis [3], they divided the iris into a greater number of concentric bands and used a genetic algorithm to determine the most distinctive ones. Hollingsworth *et al.* [4] demonstrated the existence of fragile or inconsistent bits,

which are defined as bits that have a substantial probability of changing from a 0 to a 1 or vice versa in images of the same iris. The percentage of images in which fragile bits change is the consistency threshold. Authors also found that certain bits are consistent even across out-of-focus and noisy images. This information has been exploited in systems by masking the fragile bits before the comparison stage in order to increase the identification accuracy. In their work, Rathgeb *et al.* [5] computed a reliability mask in which the reliability at each bit position was defined as the difference between the estimated probabilities of intra-class and inter-class error occurrence. Broussard *et al.* [6] and Hilal *et al.* [7] calculated the identification accuracy achieved by different iris regions in order to investigate their contribution to the match decision.

Results reported in all previous approaches seem to indicate that texture information located in the middle region of the iris code is more consistent, and the maximum consistency is reached closer to the pupillary boundary than to the limbus. More specifically, if rings are numbered from the pupillary boundary out to the limbus as 1 to 10, the best decidability values were found in [2] when using rings 2, 3, 4, 5 and 7. Using a consistency threshold of 40% for the fragile bits, best results were obtained in [4] for rings 5 to 12 out of twenty (or 2 to 6 out of ten approximately). In [6], rings 4 to 8 out of ten were reported to be the most consistent, whereas in [7], rings 2 and 3 out of ten performed the best, followed by rings 1, 4 and 5. As observed, some differences exist in those rings near the pupillary boundary. The authors themselves hypothesize about the potential effect of segmentation and normalization in their results, and such hypothesis is confirmed in [7] by comparing the results obtained for different segmentation and normalization methods.

In [4] and [6], the authors hypothesize about the effect of pupil dilation on the consistency of the inner regions of the iris, but no experiments are presented to test this hypothesis. In this work, the effect of pupil dilation and constriction on information consistency within the iris is analysed experimentally in detail. Both light-induced and drug-induced pupil dilation and constriction are considered and compared.

The problem of iris deformation and the effect of changes in pupil size on iris recognition have become

active research topics in recent years. Some authors have focused their attention on mathematically modelling the effects of iris deformation and pupil dilation. Clark *et al.* [8] propose a biomechanical model to explore the nonlinear dynamics of iris deformation. In [9], Wei *et al.* present a deformation correction method which uses a Gaussian function to model the deviation from the linear stretch. Thornton *et al.* [10] use the maximum a posteriori probability (MAP) estimate of the parameters of the deformation to define a distortion-tolerant similarity metric. Other authors have focused on experimentally demonstrating how changes in pupil size affect iris recognition performance [11]-[13]. Two of these [12], [13] discuss drug-induced pupil dilation. In order to determine how changes in pupil size affect performance, identification accuracies are compared in approaches [11]-[13] for different degrees of dilation at enrolment and at recognition. According to the results, when the degree of dilation at enrolment is similar to the degree of dilation at recognition, the best performance is obtained for highly constricted pupils, whereas the worst performance is obtained for highly dilated pupils. If the degree of dilation is quite different at enrolment and recognition, performance is severely affected regardless of the fact that the pupil is dilated or constricted. This research work is not aimed at determining how pupil dilation and constriction affect identification accuracy, but at investigating their effect on the iris code consistency by analysing which regions of the iris are more affected by such degradations, and quantifying how affected they are using the number of bit errors in the iris code. In order to do this, bit errors are first calculated for a reference database captured under normal conditions, with normal pupil sizes. Images affected by light-induced and drug-induced pupil dilation and constriction are then compared with such reference images.

In this paper, a thorough bit error analysis in different iris regions (rings and sectors) is carried out in order to investigate the effect of light and drug induced pupil dilation and constriction on the consistency of texture information within the iris. Bit error in this context is defined as the number of iris code bits that ‘flip’ from 1 to 0 or vice versa as a fraction of the total number of bits in the selected region for analysis. The details of the proposed error analysis are introduced in Section 2. Section 3 describes the methodology used to calculate the bit error distribution and the results. Conclusions are summarized in Section 4.

## 2. Distribution of bit errors within the iris

Different criteria can be used to identify the location of the most discriminatory information of the iris. Fragile bits [4], probabilities of intra-class and inter-class error occurrence [5], identification accuracy [6],[7] or decidability [7] are some of these criteria. In order to better understand the effect of medium and severe pupil dilation and

constriction on the iris texture consistency, a criterion which is closely related to the texture-level is desirable. The mean normalized number of bit errors between iris codes is the criterion selected for this article.

Any biometric system, regardless of the particular biometric trait, is basically composed of four different stages: data acquisition, pre-processing, feature extraction, and comparison. Different iris algorithms can be used to implement the different stages. The bit error analysis presented in this research is carried out after the feature extraction stage, and the binary iris codes and iris masks required to compute the bit errors are obtained from an in-house algorithm, which is described in detail in Section 3.1. It is important to note that when comparing two iris codes, iris alignment is a key issue. In this case, each code is cyclically shifted across a range of positions to simulate different rotations of the eye. The final match score is the lowest dissimilarity score across all shifted comparisons.

The normalized bit error between two iris codes  $\{\mathbf{C}_1, \mathbf{C}_2\}$  whose mask bit vectors are denoted  $\{\mathbf{M}_1, \mathbf{M}_2\}$  is defined as the number of bits that differ between the unmasked portions of the iris codes as a fraction of the total number of bits that are compared. This dissimilarity metric is also known as normalized or fractional Hamming distance. The normalized bit error is calculated as:

$$\varepsilon = \frac{|(\mathbf{C}_1 \oplus \mathbf{C}_2) \cdot (\mathbf{M}_1 \cdot \mathbf{M}_2)|}{|\mathbf{M}_1 \cdot \mathbf{M}_2|} \quad (1)$$

where  $\oplus$  and  $\cdot$  are the bitwise-XOR and the bitwise-AND operation respectively, and  $||$  represents the L1 norm.

To better characterize the distribution of the bit errors within the iris, the value of  $\varepsilon$  is computed for different iris parts defined based on the iris radius and the angle as shown in Figure 1. The iris code associated with each iris part is a fraction of the complete iris code, properly selected by masking. In the case of the radius,  $R$  different concentric rings of size  $(R_{\text{iris}} - R_{\text{pupil}})/R$  are considered, where  $R_{\text{iris}}$  and  $R_{\text{pupil}}$  are the radius of the iris and the pupil respectively. In the case of the angle,  $S$  sectors are considered. From here on, the subscripts  $r$  and  $\theta$  are used to differentiate between radial parts or rings, and angular parts or sectors. In each case, a superscript will be used to denote the specific ring ( $i = 1, \dots, R$ ) and sector ( $j = 1, \dots, S$ ), numbered as shown in Figure 1. Considering the iris partitioning,  $\varepsilon_r^i$  denotes the normalized number of bit errors in ring  $i$ , and  $\varepsilon_\theta^j$  denotes the normalized number of bit errors in sector  $j$ . Since datasets differ in the number of identities or users and the number of iris samples for each, the previously defined normalized number of bit errors per ring and sector are averaged for the number of comparisons of any given database. The mean normalized bit error per ring and sector denoted  $\bar{\varepsilon}_r^i$  and  $\bar{\varepsilon}_\theta^j$  respectively, will be used in the next section to analyse the effect of pupil dilation and constriction on the consistency of iris texture.

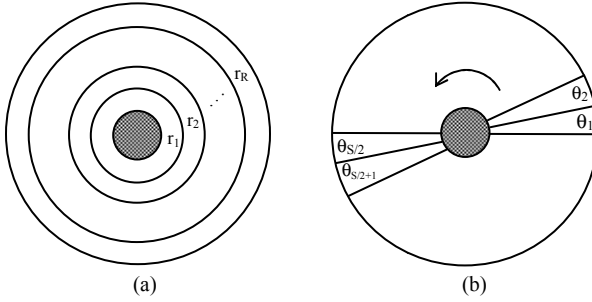


Figure 1: Iris partitioning. (a) Radial iris partitioning:  $R$  rings from pupillary boundary to iris boundary or limbus. (b) Angular iris partitioning:  $S$  sectors starting from right iris cone.

### 3. Experimental validation

#### 3.1. Iris recognition base algorithm

The implemented iris recognition base algorithm is based on Daugman's approach [14]. In the pre-processing stage, the black hole search method [15] is first used to locate the pupil (course search). A simplified version of Daugman's integro-differential operator is then used (fine search) to define the contours. In order to detect and mask the non-biometric information from the image (eyelids, eyelashes, and reflections), a combination of Canny's edge detection algorithm [16] and Deriche *et al.* algorithm [17] is used. In the feature extraction stage, convolution with 2-D Gabor filters is used to extract the texture from the normalized iris image. Taking into account the results reported by Zheng and Su in [18], only one orientation and scale are used. Filtering is performed by sectors (the normalized image is divided into 12 rings and 256 sectors per ring) and only the usable iris area is considered for normalization. Binary coding of the coefficients obtained after filtering and template matching, based on Hamming distance, are carried out as proposed by Daugman after barrel-shifting to correct iris rotation. As a result, a 3072 bits iris code is obtained. Using an in-house iris dataset composed of 354 images captured under normal conditions from 118 different iris classes, the Equal Error Rate (EER) value obtained is 0.87%, close to other state of the art results [1].

#### 3.2. Databases

Three different in-house databases are used to perform the experiments in this paper: a reference database obtained under normal conditions, and two databases made up of irises affected by medium and severe pupil dilation and constriction. Controlling the lighting conditions and instilling a mydriatic/miotic agent in the form of eye drops to the participants were the two methods selected to obtain the desired effect. The two options were considered with the purpose of analysing the differences between light-induced and drug-induced dilation and constriction.

In the case of the eye drops instillation, the data collection was assisted by an optometrist. Subjects were appropriately debriefed and signed a consent form. In order to discern different degrees of pupil dilation and constriction, the ratio between the pupil radius and the iris radius is used (see Table I). This pupil-to-iris ratio is denoted as  $\rho$ . The sensor used for the data collection is the IG-AD100, a dual eye auto-focus camera which works in the near infrared wavelength. All images were acquired at a resolution of 640x480 pixels.

The reference database includes a total of 354 iris images captured under normal conditions. Images were taken from 59 different participants, who provided 3 images for each eye. The total number of iris classes is thus 118. The second database contains 434 iris images affected by medium and severe pupil dilation. Some of the medium dilated images were obtained by turning the ambient lighting off. The infrared LEDs used by the IG-AD100 to illuminate the iris were enough to take high-quality iris images in the absence of ambient light and did not modify the pupil dilation, which is caused by the visible light. Images taken in a short time frame after the instillation of a mydriatic agent (1% tropicamide in this case) can also be categorized as medium dilated images. Severe dilation or mydriasis could only be achieved in the late stages after the instillation of the mydriatic agent. The last database includes 366 images affected by medium and severe pupil constriction. Medium pupil constriction was achieved by pointing a visible light source directly at the participant's eyes, and also in the early stages after the instillation of a miotic agent in the form of eye drops (2% pilocarpine in this case). Severe pupil constriction or miosis could only be achieved in the late stages after the instillation of the miotic agent.

The bit error analysis carried out in this paper is aimed at providing insight about bit errors that are directly related to changes in the iris texture, and should not be influenced by errors introduced owing to segmentation. In order to eliminate this problem, images from all the databases are automatically segmented and then subjected to a manual selection process to retain only those that are correctly segmented (verified by visual inspection). Although all non-biometric information was meant to be completely removed (eyelids, eyelashes, lighting artefacts, specular reflections, etc.), some minor imperfections could not be avoided. Information about the resulting databases can be found in Table I. Sample images are shown in Figure 2.

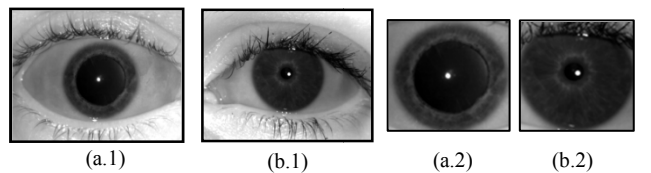


Figure 2: Sample images with details. (a) Drug-induced severe pupil dilation (b) Drug-induced severe pupil constriction.

Table I. Databases information.

Conditions		Stage	Ratio ( $\rho = R_{\text{pupil}}/R_{\text{iris}}$ )	Total images	Optimal images
Dilation	No light	Medium	$0.515 \leq \rho < 0.625$	74	41
	Drops	Medium	$0.515 \leq \rho < 0.625$	153	55
		Severe	$\rho \geq 0.625$	207	88
Constriction	Light	Medium	$0.235 < \rho \leq 0.265$	144	58
		Medium	$0.235 < \rho \leq 0.265$	117	59
	Drops	Severe	$\rho \leq 0.235$	105	43
Normal conditions (reference)			$0.265 < \rho < 0.515$	354	104

### 3.3. Reference distribution of bit errors

Using (1) it is possible to calculate the mean normalized number of bit errors between iris codes of different iris parts for any given database and algorithm. In this paper, the mean normalized bit error is computed for 12 radial parts or rings ( $\bar{\varepsilon}_r^i, i = 1, \dots, 12$ ) and 12 angular parts or sectors ( $\bar{\varepsilon}_\theta^j, j = 1, \dots, 12$ ), as defined in Figure 1. Since the iris code of the whole iris has 3072 bits, the iris code of each of the parts (rings and sectors) has 256 bits. The mean normalized bit error obtained for the optimally segmented reference subset using the base iris recognition algorithm is shown in Figure 3 for the client and impostor distributions. This result will be the reference for the rest of the paper.

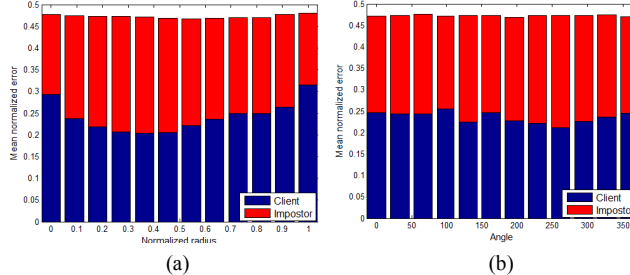


Figure 3: Mean normalized bit error as a function of the (a) radius and (b) angle for client and impostor distributions using the optimally segmented reference subset.

According to Figure 3, the distribution of bit errors obtained from impostor comparisons (red) can be considered uniform and almost equal to 0.5 for radial partitions or rings, as well as angular partitions or sectors. This result is consistent with the fact that if two irises are from different identities, they are expected to have statistically independent iris codes [19]. Since any bit in an iris code is equally likely to be a 1 or a 0, the expected fraction of agreeing bits between two independent iris codes is 0.5. It has been verified that the same behaviour is obtained for impostor comparisons in the case of pupil dilation and constriction. Since no useful information is obtained for impostors, only results obtained from client comparisons will be considered from here on.

For client comparisons (blue), rings closer to the pupil and those closer to the limbus are affected more by bit

errors than the ones in the middle. This result is consistent with those obtained by other authors mentioned in Section 1. Since all but some minor segmentation errors were eliminated to obtain this result, the reason for such behaviour can be mostly attributed to the texture differences near the boundaries, caused by differences in the iris tissue. Statistical significance tests are later performed to validate this result. With reference to sector partitioning, the mean normalized bit error is almost uniform, and the average equals 0.24 (24%). Values slightly over the mean (0.97% over on average) can be observed on the upper part of the iris ( $\theta = [0^\circ, 180^\circ]$ ), where occlusions due to the upper eyelid and eyelashes are common. The lowest number of bit errors (1.3% under the mean on average) can be observed on the lower part of the iris. These small fluctuations are mainly due to the minor imperfections residual after manual selection of images free from segmentation errors.

In order to validate the previous result and obtain statistical confidence, repeated random sub-sampling based validation is used. Half of the iris samples from the optimally segmented reference subset are randomly selected and 100 such Monte Carlo trials are used to compute statistics. Results are shown in Figure 4 with the standard deviation for each ring/sector represented as an error bar above and below the mean value. Results show that the maximum standard deviation when considering radial partitioning occurs for the outer ring (the nearest to the limbus) and is equal to 1.5%. The mean value for the standard deviation is 0.88%. In the case of angular partitioning, a maximum standard deviation of 1.1% occurs for angles around  $90^\circ$  (third sector). This value is not far from the mean value for the standard deviation, which equals 0.91%.

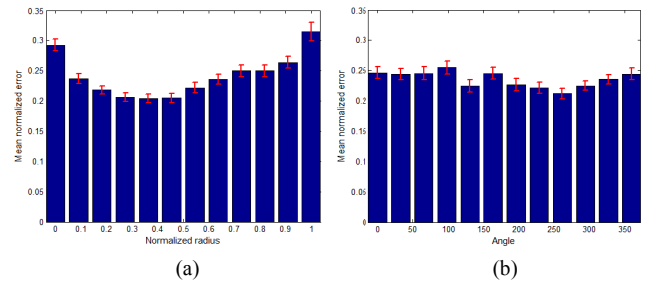


Figure 4: Mean normalized bit error as a function of the (a) radius and (b) angle for client comparisons using the optimally segmented reference subset. Error bars are one standard deviation.

The V-shaped trend for radial partitions or rings appears to be statistically significant, and any deviation from a uniform error distribution for angular partitions or sectors is not statistically significant. Considering its relevance in this study, statistical significance testing will be used to validate these results. First of all, a Lilliefors test [20] is applied to test the null hypothesis that bit errors from each ring and

sector come from a normally distributed population. The normality of the bit error data of each ring is confirmed (mean p-value equals 0.3405), whereas the normality of the bit error data of each sector is rejected. Since the bit error data in each ring is normally distributed, the 3-sigma test is performed for all rings. According to this test, 99.73% of the bit error values lie within the 3-sigma error bars represented in Figure 5(a). Results show that the V-shaped trend initially assumed can be accepted as significant, since any curve to fit the bit error data within the 3-sigma error bars will exhibit a lower number of bit errors in the middle region of the iris, and a higher number in the areas nearer the pupil and the limbus. Since bit error data does not fit a normal distribution in the case of sectors, an alternative way to test statistical significance has been considered. Based on the 100 Monte Carlo trials performed, the error bars that enclose 90% of the bit error values have been calculated and are shown in Figure 5(b). According to the results, a null hypothesis that the bit errors are uniformly distributed as a function of the angle cannot be ruled out because it is possible for such a curve to be within the error bars. However there is some fluctuation around 120 degrees which can be significant at a lower level of confidence. This may be arising from the minor imperfections that remain in the trimmed dataset free of segmentation errors.

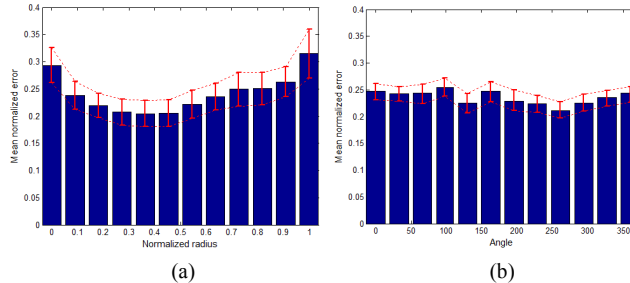


Figure 5: Statistical significance testing of reference distribution of bit errors. (a) 3-sigma test performed for each ring. (b) 90% confidence test performed for each sector.

### 3.4. Effect of pupil dilation and constriction

#### A. Effect of pupil dilation

To analyse the effect of pupil dilation on the iris texture information, the mean normalized bit error is computed as a function of the iris radius and angle. For analysis purposes, the difference between the bit error distributions corresponding to the three cases under study (severe drug-induced dilation, medium drug-induced dilation, and medium light-induced dilation) is shown in Figure 6.

In agreement with previously reported results, the graphs in Figure 6 clearly show that significant pupil dilation considerably increase the number of bit errors. Since pupil dilation reduces the amount of iris area visible, there is less information (fewer pixels) to characterize the texture of the

iris. This increases the number of bit errors. By comparing light-induced (cyan) and drug-induced (green) pupil dilation within the same range of pupil-to-iris ratio, it can be observed that more bit errors occur for the latter. On average, a 3.5% bit error increase can be observed in the radial and angular cases for drug-induced dilation compared to light-induced dilation. This result can be explained by the fact that mydriatic agents act by paralyzing the iris muscles, so their effect on the iris texture is more severe than the effect provoked by the absence of light.

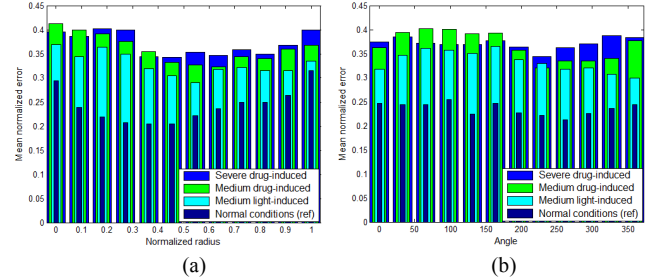


Figure 6: Difference between mean normalized bit error as a function of the (a) radius and (b) angle, calculated from client comparisons using the optimally segmented images of the reference and dilation-related datasets.

In order to gauge statistical confidence of the previous result, repeated random sub-sampling based validation is used. Repeating the same steps performed when analysing the reference bit error distribution, 100 Monte Carlo trials are used with 50:50 split of the images. The result obtained when comparing medium light-induced and medium drug-induced pupil dilation can be seen in Figure 7, with error bars showing the one standard deviation intervals.

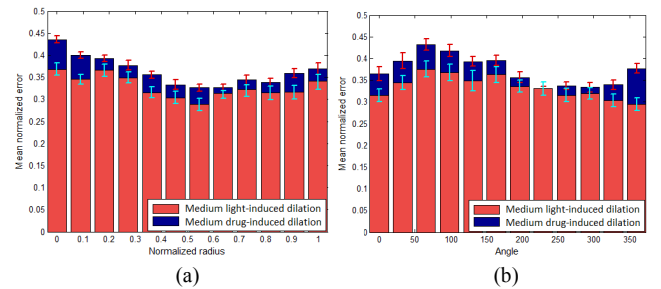


Figure 7: Difference between mean normalized bit error as a function of the (a) radius and (b) angle, calculated from client comparisons using the optimally segmented images from the medium light-induced and medium drug-induced pupil dilation subsets. Standard deviation is shown as error bars.

According to the results, error bars do not overlap in the case of radial partitions or rings, so the difference between light-induced and drug-induced dilation in such case can be considered statistically significant with one standard deviation confidence level. The fact that rings closer to the pupil show a bigger difference correlates well with the fact that the mydriatic agent instilled to the users (1% tropicamide)

affect the pupillary area more severely than the rest of the iris. When the iris is divided into angular parts or sectors, the effects of light-induced and drug-induced pupil dilation are not observed to be statistically significantly different for all sectors. It may be noted that dilation is induced by drugs or exposure to darkness, and there is no good reason for any light-related directional dependence arising from it.

Figure 8 shows the bit error distribution obtained for medium and severe pupil dilation, together with the one standard deviation intervals. The reference bit error distribution is represented in each graph as a red/blue line. Light-induced and drug-induced medium pupil dilation subsets have been combined with the objective of increasing the degrees of freedom and make the results more reliable.

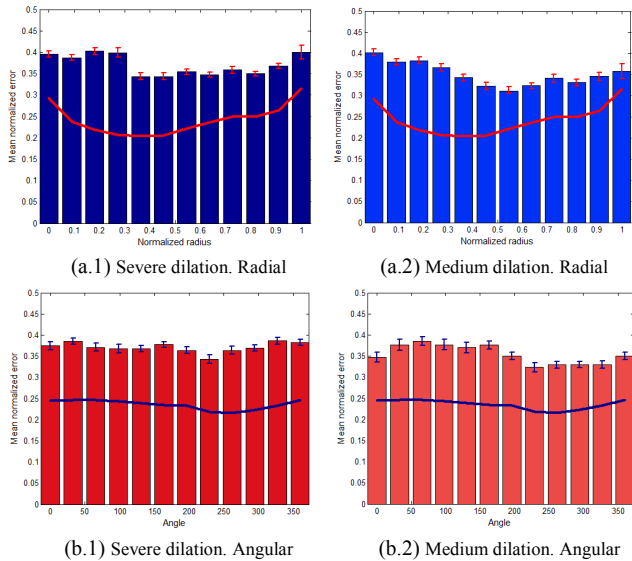


Figure 8: Mean normalized bit error as a function of the radius for (a.1) severe and (a.2) medium dilation, and mean normalized bit error as a function of the angle for (b.1) severe and (b.2) medium dilation. Data obtained from client comparisons using optimally segmented subsets. Standard deviation is shown as error bars. Reference bit error distribution is represented as a red/blue line.

According to Figure 8 (a.1), the V-shaped trend obtained under normal conditions for radial partitions or rings disappears when the iris is affected by severe pupil dilation. Due to the small amount of iris area visible and the loss of texture information, bit errors are distributed in a more uniform way, although the four rings nearer to the pupil are clearly more affected by the dilation and show an increased number of errors. In the case of medium pupil dilation (Figure 8 (a.2)), the original V-shaped trend is not totally lost, but slightly displaced towards more outer rings of the iris. This displacement is due to the fact that the inner rings are still severely affected by the dilation, whereas the outer rings of the iris are less affected than in the case of severe dilation. The distribution of bit errors for angular partitions

or sectors shown in Figure 8 (b.1) and (b.2) are quite uniform regardless of the degree of dilation. Similar to the behaviour observed under normal conditions, a slight increase in the number of bit errors can be observed in sectors between 50 and 150 degrees. This may be arising from the minor imperfections that remain in the trimmed databases free of segmentation errors. On average, the bit error increase with respect to the reference is 13.2% for severe pupil dilation and 11.7% for medium pupil dilation.

### B. Effect of pupil constriction

The final part of this paper is aimed at analysing the effect of pupil constriction on the bit error distribution. The difference between the bit error distributions corresponding to the three cases under study (severe drug-induced constriction, medium drug-induced constriction, and medium light-induced constriction) can be seen in Figure 9.

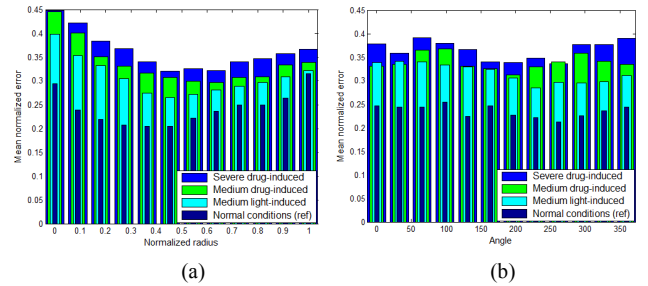


Figure 9: Difference between mean normalized bit error as a function of the (a) radius and (b) angle, calculated from client comparisons using the optimally segmented images of the reference and constriction-related datasets.

The increase in the number of bit errors shown in Figure 9 is due to the fact that some of the texture information that becomes available when the pupil constricts is not available in the reference images, which are captured under normal conditions and show normal pupil sizes. On average, the bit error increase with respect to the reference is 12.6% for severe pupil constriction and 8.9% for medium pupil constriction. Again, drug-induced errors (green) are higher than light-induced (cyan) for the same range of pupil-to-iris ratio (2.7% higher on average). The effect of the miotic agent on the iris muscles is the cause of this. Statistical confidence of the previous result has been tested and results of the comparison between medium light-induced and medium drug-induced pupil constriction are shown in Figure 10, with error bars showing the one standard deviation intervals. According to the results, error bars do not overlap when considering radial partitions or rings except for rings closest to the limbus. The difference between light and drug induced constriction can be considered significant with one standard deviation confidence level for rings close to the pupil and well into the middle region. Unlike the case of pupil dilation, where a very noticeable difference between light and drug induced

dilation could be observed for rings near the pupil, the difference between light and drug induced constriction is quite similar for all rings. This result indicates that the miotic agent instilled to the users (2% pilocarpine) does not affect the pupillary area as severely as the mydriatic agent (1% tropicamide). In the case of angular partitions or sectors, the difference between light and drug induced pupil constriction is not statistically significant for most sectors. However, for a few sectors closer to the limbus there is a significant difference, the reasons for which are not clear. Directionality arising from a dominant direction for the light-induced stimulation cannot be ruled out.

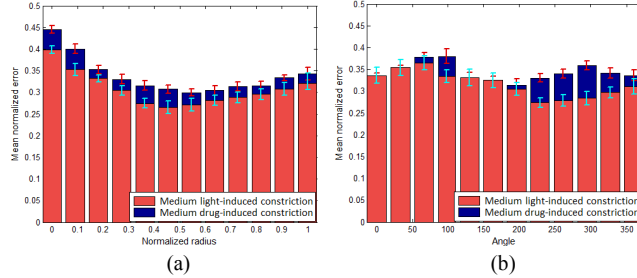


Figure 10: Difference between mean normalized bit error as a function of the (a) radius and (b) angle, calculated from client comparisons using the optimally segmented images from the medium light-induced and medium drug-induced pupil constriction subsets. Standard deviation is shown as error bars.

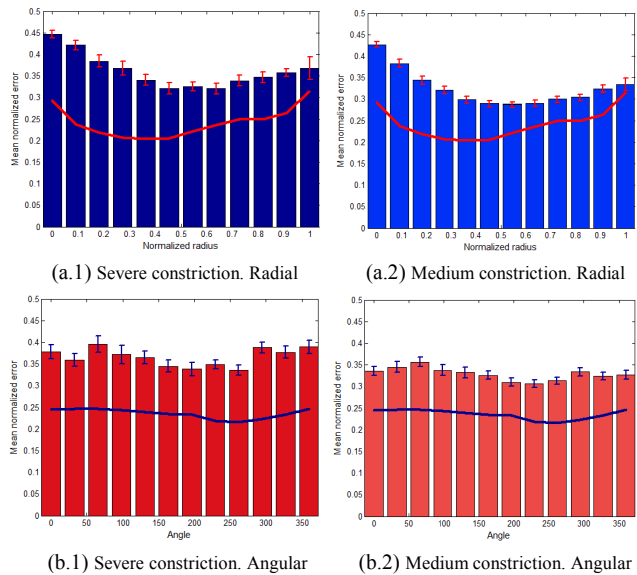


Figure 11: Mean normalized bit error as a function of the radius for (a.1) severe and (a.2) medium constriction, and mean normalized bit error as a function of the angle for (b.1) severe and (b.2) medium constriction. Data obtained from client comparisons with optimally segmented subsets. Standard deviation is shown as error bars. Reference bit error distribution represented as a red/blue line.

Figure 11 (a.1) and (a.2) interestingly show that for severe and medium pupil constriction, the radial bit error

distributions retain characteristics of the V-shaped trend of the reference data, although they get stretched up near the pupil. Figure 11 (b.1) and (b.2) show that bit errors as a function of the angle increase but retain the uniform distribution within limits of statistical fluctuation.

Figure 11 for pupil constriction is analogous to Figure 8 for pupil dilation. The most important difference is that as a function of the radius, the errors retain a decreasing trend from the pupil outwards and do not tend towards uniform as in Figure 8. The average increase of bit errors in the case of pupil dilation is higher than in the case of pupil constriction (13.2% vs. 12.6% in final stages, and 11.7% vs. 8.9% in medium stages), although rings closer to the pupil are more affected by constriction (45% maximum according to Figure 11 compared to 41% maximum in Figure 8).

## 4. Conclusions

Bit errors in the iris code are systematically analysed in this paper for light and drug induced pupil dilation and constriction, and compared to reference iris images with normal pupil sizes. Results show that:

1. For all cases, the main increase in the number of errors occurs closer to the pupil.
2. Pupil dilation causes more errors than pupil constriction on average, although rings closer to the pupil are more affected by pupil constriction.
3. The bit error distribution as a function of the radius shows a decreasing trend from the pupil outwards for pupil constriction; it tends to become more uniform for pupil dilation. The bit error distribution as a function of the angle is quite uniform in both cases.
4. Light-induced pupil dilation/constriction is different than drug-induced pupil dilation/constriction. It causes fewer bit errors.

The results presented can be useful in applications such as (a) biometric cryptography where keys could be extracted based on bits of the iris coming from selected rings or sectors, (b) cancellable biometric signatures for privacy protection where only selected bits from the iris may be used and (c) performance improvement of iris recognition systems that use partial iris images.

## References

- [1] P. J. Grother, G. W. Quinn, J. R. Matey, M. L. Ngan, W. J. Salamon, G. P. Fiumara, and C. I. Watson. IREX III - Performance of iris identification algorithms. NIST Interagency/Internal Report (NISTIR) 7836, 2012.
- [2] M. B. Pereira and A. C. P. Veiga. A method for improving the reliability of an iris recognition system. IEEE Pacific Rim Conference on Communications, Computers and Signal Processing, pp. 665–668, 2005.
- [3] M. B. Pereira and A. C. P. Veiga. Application of genetic algorithms to improve the reliability of an iris recognition system. Workshop on Machine Learning for Signal Processing, pp. 159–164, 2005.

- [4] K. P. Hollingsworth, K. W. Bowyer, and P. J. Flynn. The best bits in an iris code. *IEEE Transactions on Pattern Analysis and Machine Intelligence*, 31(6): 964–973, 2009.
- [5] C. Rathgeb, A. Uhl, and P. Wild. Incremental iris recognition: A single-algorithm serial fusion strategy to optimize time complexity. *IEEE International Conference on Biometrics: Theory Applications and Systems*, pp.1–6, 2010.
- [6] R. P. Broussard, L. R. Kennell, and R. W. Ives. Identifying discriminatory information content within the iris. *Biometric Technology for Human Identification*, 2008.
- [7] A. Hilal, P. Beauseroy, and B. Daya. Identifying discriminatory characteristics location in an iris template. *Advances in Systems Science. Advances in Intelligent Systems and Computing*, 240: 183–193, Springer, 2014.
- [8] A. D. Clark, S. A. Kulp, I. H. Herron, and A. A. Ross. Exploring the nonlinear dynamics of iris deformation. *Biometric Consortium Conference*, 2011.
- [9] Z. Wei, T. Tan, and Z. Sun. Nonlinear iris deformation correction based on Gaussian model. *Advances in Biometrics, Lecture Notes in Computer Science*, Springer, 4642: 780–789, 2007.
- [10] J. Thornton, M. Savvides, and V. Kumar. A Bayesian approach to deformed pattern matching of iris images. *IEEE Transactions on Pattern Analysis and Machine Intelligence*, 29: 596–606, 2007.
- [11] K. Hollingsworth, K. Bowyer, and P. Flynn. Pupil dilation degrades iris biometric performance. *Computer Vision and Image Understanding*, 113(1):150–157, 2009.
- [12] L. Dhir, N. E. Habib, D. M. Monro, and S. Rakshit. Effect of cataract surgery and pupil dilation on iris pattern recognition for personal authentication. *Eye*, 224(6):1006–1010, 2010.
- [13] O. Seyeddain, H. Kraker, A. Redlberger, A. K. Dexl, G. Grabner, and M. Emesz. Reliability of automatic biometric iris recognition after phacoemulsification or drug-induced pupil dilation. *European Journal of Ophthalmology*, 24(1):58–62, 2014.
- [14] J. G. Daugman. High confidence visual recognition of persons by a test of statistical independence. *IEEE Transactions on Pattern Analysis and Machine Intelligence*, 15(11):1148–1161, 1993.
- [15] C. C. Teo and H.T. Ewe. An efficient one-dimensional fractal analysis for iris recognition. *International Conference on Computer Graphics, Visualization and Computer Vision*, 157–160, 2005.
- [16] J. Canny. A Computational approach to edge detection. *IEEE Transactions on Pattern Analysis and Machine Intelligence*, 8(6):679–698, 1986.
- [17] R. Deriche, J. P. Cocquerez, and G. Almouzni. An efficient method to build early image description. *International Conference on Pattern Recognition*, 1988.
- [18] H. Zheng and F. Su. An improved iris recognition system based on Gabor filters. *IEEE International Conference on Network Infrastructure and Digital Content*, pp. 823–827, 2009.
- [19] J. Daugman. The importance of being random: statistical principles of iris recognition. *Pattern recognition*, 36(2):279–291, 2003.
- [20] H. W. Lilliefors. On the Kolmogorov-Smirnov test for normality with mean and variance unknown. *Journal of the American Statistical Association*, 62(318):399–402, 1967.